Xiong, C., Lühr, H., Stolle, C. (2014): Seasonal and latitudinal variations of the electron density nonmigrating tidal spectrum in the topside ionospheric F region as resolved from CHAMP observations. - *Journal of Geophysical Research*,*119*, 12, p. 10,416-10,425.

DOI: http://doi.org/10.1002/2014JA020354

AGU PUBLICATIONS

JGR

Journal of Geophysical Research: Space Physics

RESEARCH ARTICLE

10.1002/2014JA020354

Key Points:
- Diurnal tides DE1,D0, and DW2 appear preferably at middle and high latitudes
- At equatorial region the most prominent tides are DE2 and DE3
- D0 exhibits antiphase variations between the two hemispheres

Correspondence to:
C. Xiong,
bear@gfz-potsdam.de

Citation:
Xiong, C., H. Lühr, and C. Stolle (2014), Seasonal and latitudinal variations of the electron density nonmigrating tidal spectrum in the topside ionospheric *F* region as resolved from CHAMP observations, *J. Geophys. Res. Space Physics*, *119*, 10,416–10,425, doi:10.1002/2014JA020354.

Received 1 JUL 2014
Accepted 19 NOV 2014
Accepted article online 25 NOV 2014
Published online 12 DEC 2014

Seasonal and latitudinal variations of the electron density nonmigrating tidal spectrum in the topside ionospheric *F* region as resolved from CHAMP observations

Chao Xiong[1,2], Hermann Lühr[1], and Claudia Stolle[1]

[1]Helmholtz Centre Potsdam, GFZ German Research Centre for Geosciences, Potsdam, Germany, [2]Department of Space Physics, College of Electronic Information, Wuhan University, Wuhan, China

Abstract In this study we present for the first time the nonmigrating tidal spectrum for the electron density in the topside ionosphere on global scale for different seasons at both solar maximum and minimum conditions. The electron density observations from the CHAMP (CHAllenging Minisatellite Payload) satellite provide evidence for prominent nonmigrating tides at different latitude regions. At middle and high latitudes the most prominent diurnal tides are DE1, D0, and DW2, as well as semidiurnal tides SW1 and SW3 preferably during equinox seasons. DE1 is only found in the northern middle and high latitudes, while D0 and DW2 are much stronger in the Southern Hemisphere. These tides are believed to be driven by the thermospheric winds through ion-neutral interactions. At equatorial and low-latitude regions the most prominent diurnal tides are DE2 and DE3. DE2 is found to be present at low-latitude regions throughout the whole year with larger amplitudes in the Southern Hemisphere, while DE3 shows largest amplitudes (symmetric above the dip equator) at the equatorial ionization anomaly (EIA) crest region during September equinox. A general antiphase behavior between the EIA crest and trough is observed for the tides DE3, DE2, DW2, and SW3. We consider this as strong evidence for the modulation of the EIA electron density by the *E* layer zonal electric field via the ion fountain effect. An exception is the tidal component D0, which exhibits antiphase variations between the two hemispheres. The phase value at the equatorial trough is halfway between those of the two hemispheres. Presently, we cannot give an explanation for it, and study concerning special model effort is further needed.

1. Introduction

The ionosphere-thermosphere (IT) system represents the transition region between Earth's atmosphere and space. The variability of the global IT system is believed to be associated with lower atmosphere processes. In the past decade, an increasing number of studies were focusing on the longitudinal patterns of the upper atmosphere [e.g., *Immel et al.*, 2006; *Oberheide et al.*, 2006; *Lühr et al.*, 2008; *Hagan et al.*, 2009; *Häusler and Lühr*, 2009; *Wan et al.*, 2010]. Best known are the longitudinal wave number 4 (WN4) and wave number 3 (WN3) patterns at the equatorial and low-latitude regions during the months around August and solstice seasons, respectively. This WN4/WN3 patterns are considered to be associated with the eastward propagating nonmigrating tides DE3/DE2, which are excited in the troposphere by latent heat release in deep convective tropical clouds [*Hagan and Forbes*, 2002; *Oberheide et al.*, 2006; *Wan et al.*, 2010]. These nonmigrating tides propagate upward and modulate the *E* layer electric fields [*Lühr et al.*, 2008; *England et al.*, 2010]. By dynamo effects they thus cause the longitudinal wave patterns of different ionospheric quantities in the *F* region, such as the equatorial ionization anomaly (EIA), vertical plasma drift, *F* region dynamo current, and total electron content (TEC) [*Immel et al.*, 2006; *Kil et al.*, 2007; *Park et al.*, 2010; *Scherliess et al.*, 2008; *Lühr et al.*, 2012]. Direct propagation of upward propagating tides can also contribute to the longitudinal variability of IT quantities [e.g., *England et al.*, 2009; *Hagan et al.*, 2009; *Häusler and Lühr*, 2009]. Model simulations further revealed that nonlinear interaction between the migrating tides (DW1) and DE3/DE2 can lead to prominent stationary planetary waves SPW4/SPW3, with amplitudes almost equal to DE3/DE2 [*Hagan et al.*, 2009; *Oberheide et al.*, 2011; *Pancheva et al.*, 2012]. This has been confirmed especially for the equatorial electrojet (EEJ) observations by *Lühr and Manoj* [2013]. The importance of the SPW4/SPW3 contributing to the WN4/WN3 patterns in the EIA has also been reported by *Xiong and Lühr* [2013], based on in situ electron density observations from CHAllenging Minisatellite Payload (CHAMP) as well as Gravity Recovery and Climate experiment (GRACE) satellite missions.

In the context of classical tidal theory, solar thermal tides refer to those global-scale oscillations with periods determined by the motion of the Sun relative to the rotating Earth. *Jones et al.* [2013] extended the definition of tides by characterizing all Fourier components that project onto tidal periods. These tides encompass the tidal components excited by thermal sources, stationary planetary wave-tide [e.g., *Angelats i Coll and Forbes*, 2002], tide-tide interactions [*Hagan et al.*, 2009; *Oberheide et al.*, 2011], and the in situ thermospheric wind-ion drag interactions [*Jones et al.*, 2013]. All that gives rise to a spectrum of the tidal components. In accordance with previous definitions, we use the common nomenclature for labeling the tidal components in the present study. The first letter D, S, or T stands for diurnal, semidiurnal, or terdiurnal; the second letter E or W for eastward or westward propagating; and the final number quantifies the azimuthal wave number. D0 represents a wave that is increasing and decreasing simultaneously at all longitudes with a diurnal period. Stationary planetary waves are labeled as SPWs and the number at the end quantifies the number of maxima around the globe. The phase of the tides defines the time when the wave crest passes the 0° longitude meridian, while in case of SPWs the longitude of the wave maximum is given.

By using in situ electron density observations from CHAMP and GRACE satellites, our recent work revealed that the electron density of the midlatitude summer night anomaly (MSNA) exhibits prominent longitudinal wave 1 and wave 2 patterns in the Southern and Northern Hemispheres, respectively [*Xiong and Lühr*, 2014]. We further interpreted the southern MSNA, also known as Weddell Sea anomaly (WSA) as caused by a simultaneous constructive interference of the tidal components D0, DW2, as well as stationary planetary wave SPW1, while the northern MSNA can be related to the tides DE1, D0, and DW2. A similar eastward propagating wave 1 pattern of the southern MSNA has earlier been reported by *Chen et al.* [2013], by using the SAMI3 (Sami3 is Also a Model of the Ionosphere) model combined with the Thermosphere-Ionosphere Electrodynamics General Circulation Model (TIEGCM) and the Global-Scale Wave model simulations. They found that the tidal component D0 in combination with SPW1 dominate the vertical neutral wind, manifesting the southern MSNA. Further model simulations from *Jones et al.* [2013] showed that at low and middle latitudes the nonmigrating tides including DE1, D0, and DW2 could be generated in situ through ion-neutral interactions due to the longitude dependent ionosphere imposed by the magnetic field configuration.

In spite of the numerous regional studies on tidal signatures there is a global view missing of the tidal distribution in the *F* region. The aim of this study is thus to fill that gap. Based on electron density measurements from the CHAMP satellite, this paper provides tidal spectra on global scale. We aim at identifying the various generation processes at the different latitudes. This attempt is further supported by considering also possible dependence of the spectra on season and solar activity. In the sections to follow we will first introduce the data set and processing approach in section 2. Then we present the seasonal and latitudinal variations of the nonmigrating tidal spectrum from CHAMP electron density observations. In section 4 we compare our results with EEJ observations at the *E* layer and model simulations.

2. Data Sets and Processing Approach

2.1. Data Set

In this study we use the in situ electron density measurements from the CHAMP satellite focusing on the ionospheric *F* region. The CHAMP satellite was launched on 15 July 2000 into a circular, near-polar orbit (inclination: 87.3°) with an initial altitude of 456 km. By the end of the mission, 19 September 2010, the orbit had decayed to 250 km. The local time of the orbital plane changes by 1 h in 11 day, requiring about 131 days for covering all local times [*Reigber et al.*, 2002]. The Planar Langmuir Probe (PLP) on board the satellite was taking measurements of the electron density and temperature every 15 s. The PLP electron density readings are the prime data set used here, and they have been validated by comparison against digisonde measurements at Jicamarca [*McNamara et al.*, 2007]. The CHAMP electron density data (product identifier CH-ME-2-PLP) is available at the Information System and Data Center (ISDC) of the GFZ, German Research Centre for Geosciences.

2.2. Processing Approach

Our aim is to determine the global distribution of the tidal spectrum. In order to achieve that the data are divided into latitude bands and independent tidal analyses are applied to each band. The CHAMP data are sorted into 37 overlapping bands of 10° magnetic latitude width. These 37 data sets are the basis for the global spectra. Longitudinal wave structures observed by near-polar orbiting satellites can be caused by

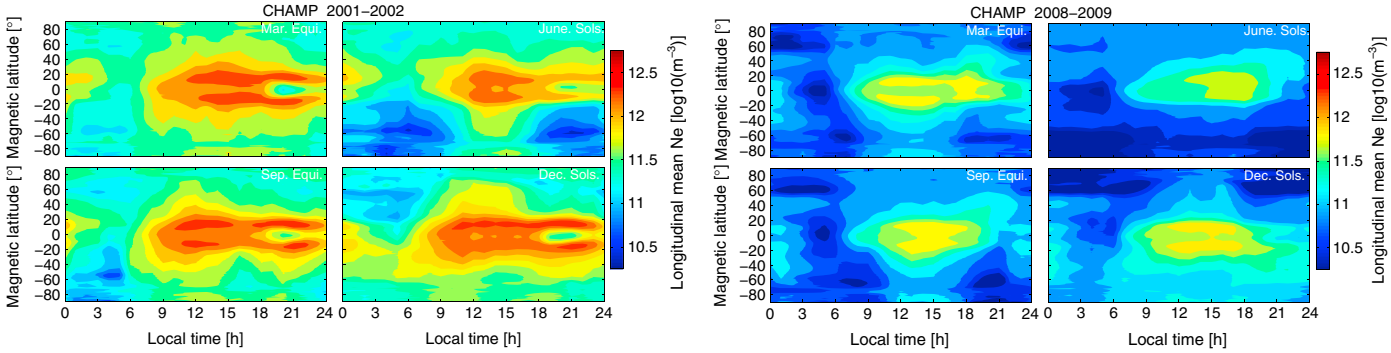

Figure 1. The magnetic latitude and local time distributions of the electron density for four seasons during (left) solar maximum and (right) solar minimum periods.

many different tidal components. A general mathematical formulation of the relation between longitudinal patterns in satellite observations and the nonmigrating tidal description in the Earth-fixed frame is given by *Forbes et al.* [2006] and by *Häusler and Lühr* [2009] in their section 2. In this study, the electron density measurements from CHAMP are first sorted into local time (1 h) by geographic longitude (15°) bins. For each latitude band, we use the following approach to separate the different tidal components. First, the longitudinal mean value has to be subtracted hour by hour to suppress the migrating tides. Then these mean-free data are processed by a Fourier transform, in order to obtain the longitudinal patterns for each wave number up to 4. In a next step a tidal wave model is fitted to the longitudinal patters. From that we derive the amplitudes and phases of all tidal components within the bandwidth of interest. For validating our decomposition approach we check the residuals, which are defined as the observations minus the synthetic signals, for systematic patterns. If no or small systematic pattern appears from the comparison, the synthetic signals are considered reliable. A similar approach has been used by *Xiong and Lühr* [2013, 2014] for investigating the tidal signatures of the EIA and MSNA.

3. Results

For our analysis we had 10 year of CHAMP electron density readings at our disposal. This covers the time from the solar maximum to the recent deep and prolonged solar minimum. In order to avoid a confusion of solar activity dependence with other tidal characteristics the whole data set has not been treated in one run. Two time intervals from 2001 to 2002 (mean $F_{10.7} = 180$ sfu) (solar flux unit (1 sfu = 10^{-22} W m^{-2} Hz^{-1})) and from 2008 to 2009 (mean $F_{10.7} = 70$ sfu) have been selected for representing solar maximum and minimum conditions. Since we know that the tidal signature in the upper atmosphere shows seasonal dependence [e.g., *Lühr et al.*, 2012], for each of the two time periods the CHAMP observations have been further divided into four seasons, centered on March equinox, June solstice, September equinox, and December solstice. For each season, overlapping periods of 131 days are needed to cover all 24 local time hours. Days with $Ap > 30$ are excluded to reduce the influence of severe magnetic disturbances.

Figure 1 presents the magnetic latitude (MLAT) in quasi-dipole coordinate [*Emmert et al.*, 2010] versus local time (LT) distributions of the electron density during solar maximum (left) and solar minimum (right) periods. Data are averaged over all longitudes. The longitudinal mean values of the electron density reflect the diurnal variation (migrating tidal components). As can be seen, the electron density is much larger for the four seasons at all latitudes and all local times during solar maximum than during solar minimum. When calculating global bin averages we obtain for the electron densities during solar maximum (minimum) for the seasons March equinox, June solstice, September equinox, and December solstice 6.67, 4.32, 5.86, and $6.29 \cdot 10^{11}$ m^{-3} (1.58, 1.24, 1.53, and $1.84 \cdot 10^{11}$ m^{-3}), respectively. A large reduction (about a factor of 4) of the mean electron density is observed although the CHAMP orbit altitude had decayed as the solar cycle declined. During the first period CHAMP was cruising at 418 km on average and at 324 km altitude during the second period. All these results confirm that the electron density in the topside *F* region reduced a lot during the recent solar minimum.

In general the electron density shows diurnal minimum and maximum between 0300–0600 LT and 1200–1500 LT for both solar activity periods, respectively. A second electron density maximum appears

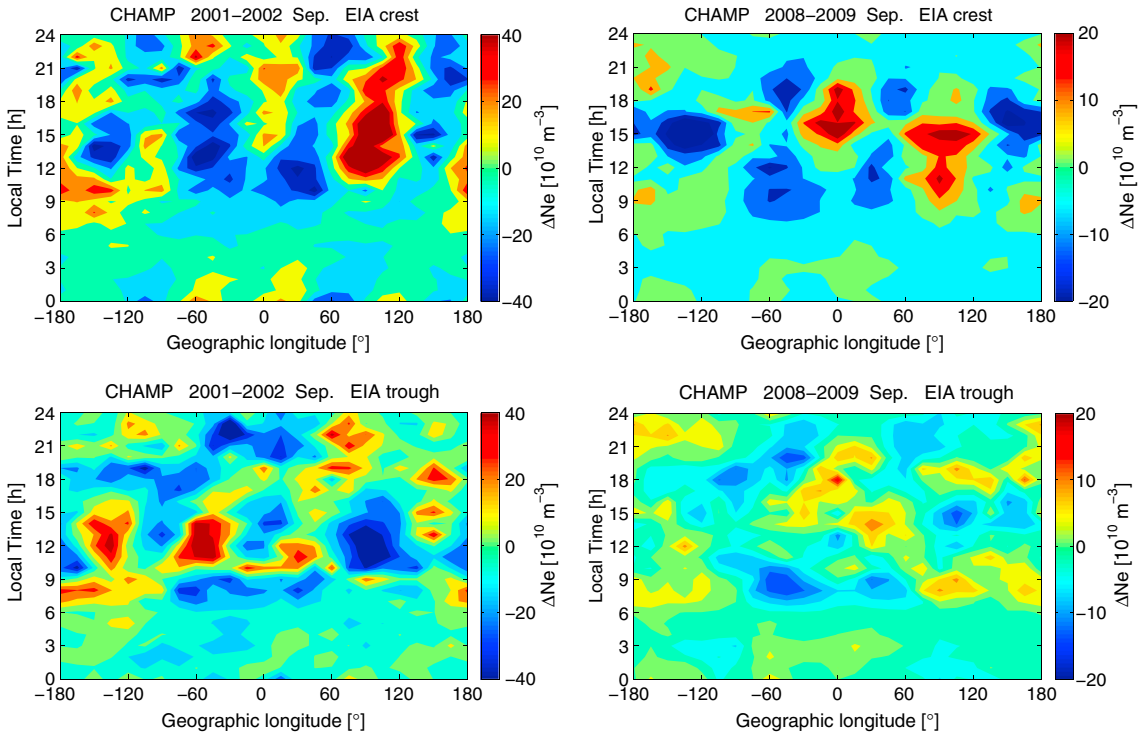

Figure 2. Local time and longitude distributions of the electron density at (top) EIA crest and (bottom) trough regions during September for (left) solar maximum and (right) solar minimum periods.

at the EIA crest region between 1800 and 2100 LT during solar maximum, coinciding with the time of the prereversal enhancement (PRE) [e.g., *Woodman*, 1970; *Fesen et al.*, 2000]. The PRE is defined as a sharp increase in vertical ion drift after sunset via an enhancement of the eastward electric field strength in the *F* region. The increased E×B drift will cause an electron density trough above the dip equator. From Figure 1, we can see that the electron densities are generally symmetric about the dip equator during PRE for all the four season during solar maximum period, with smaller magnitude during June solstice. Another interesting feature during June solstice is that the electron density is much larger in the Northern Hemisphere after 2100 LT. During solar minimum periods a PRE effect is hardly observed.

As outlined in the previous paragraph, the EIA characteristics depend strongly on local time. This is mainly due to the dependence on eastward electric field. In order to visualize this effect in more detail we have presented in Figure 2 the local time versus longitude distributions of the electron density at EIA crest (top) and trough (bottom) regions. As an example, the 131 days centered on 1 September are chosen. Latitudinal bands of 10° in magnetic latitude centered on the two crests of the EIA are merged. Prominent longitudinal features are the WN4 patterns during 0900–0200 LT (1000–2100 LT) for solar maximum (minimum) conditions. Interestingly, the longitudinal WN4 pattern is also prominent at the EIA trough regions during solar maximum, and it is out of phase compared with the EIA crest region. While during the solar minimum period, no clear WN4 pattern can be found at the EIA trough region.

As already introduced in section 2, for deriving the nonmigrating tidal signatures on global scale, we first sort the data into 37 overlapping bands of 10 magnetic latitude width. For every latitudinal band, we apply the described approach to separate the different tidal and stationary components. In this way the amplitudes and phases of the nonmigrating tides at all latitudes can be derived. Figure 3 presents in each frame the amplitudes of the stationary planetary waves (top left), diurnal (top right), semidiurnal (bottom left), and terdiurnal (bottom right) nonmigrating tides separately for the four seasons, with positive wave number referring to westward. The left column presents results from solar maximum and the right from solar minimum periods. Generally, the tidal and stationary components including SPW1, DE1, D0, DW2, SW1, and SW3 are found to have large amplitudes throughout the whole year, although showing prominent seasonal and latitudinal variations. The components SPW3 and DE2 can also be found with reduced amplitudes throughout the whole year (more prominent during solstice seasons). During September

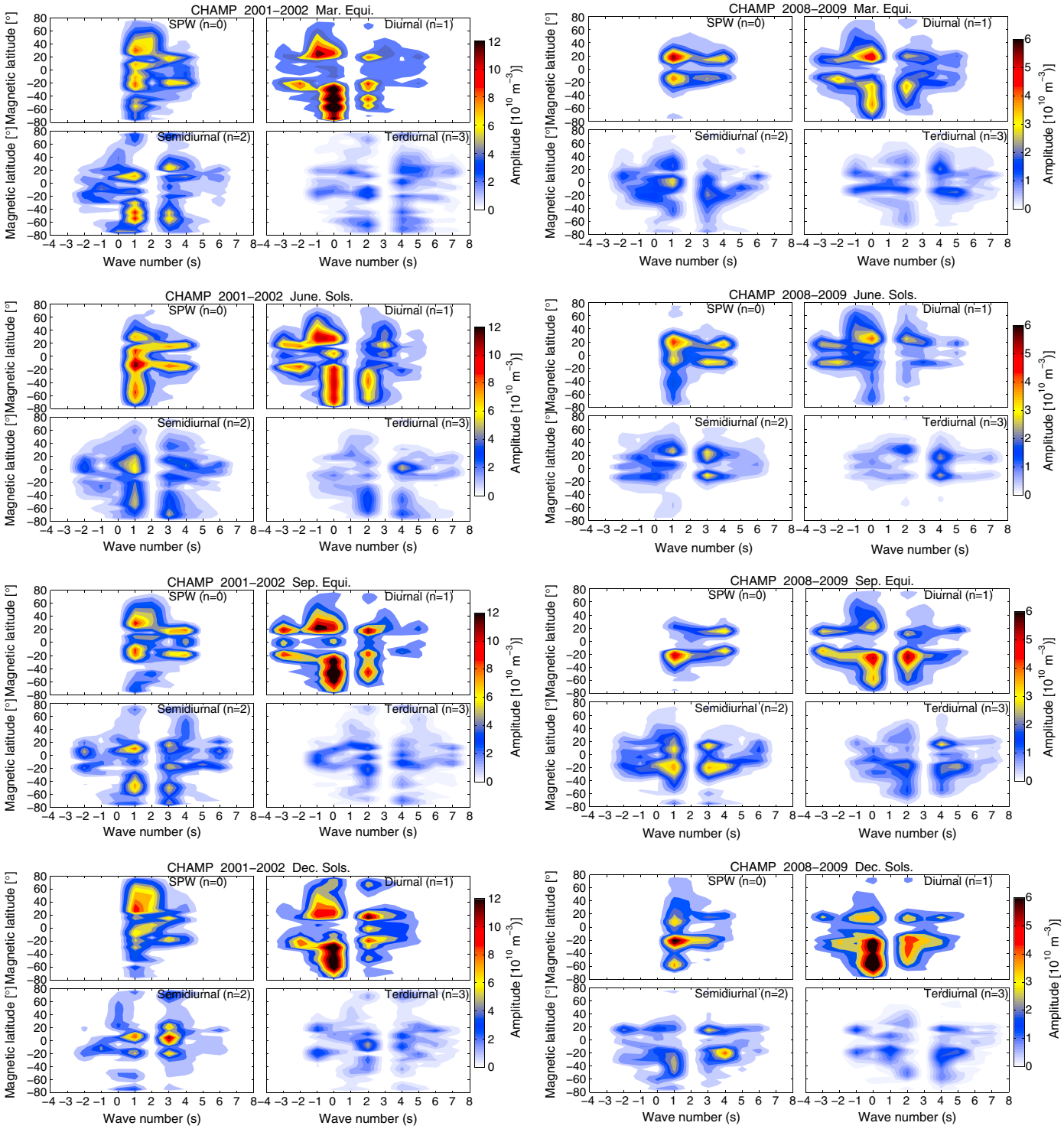

Figure 3. The latitudinal variation of the electron density tidal spectrum for the components (top left) stationary planetary wave, (top right) diurnal, (bottom left) semidiurnal and (bottom right) terdiurnal tides at *F* region altitude for the four seasons during (left column) solar maximum and (right column) minimum periods. The positive wave number refers to westward, and the scale of tidal amplitudes is different for the two solar periods.

equinox the well-known tide DE3 is found to be very prominent at the equatorial and low-latitude regions, and SPW4 as well as SE2 also show their largest amplitudes at that season. The terdiurnal tides show rather small amplitudes during all the seasons, in particular during high-activity periods. An exception is TW4 in June solstice around solar minimum. We will revisit this topic in section 4.1.

Besides the seasonal variation the nonmigrating tides also show different latitudinal dependence. There seems to be a distinction between low and middle latitudes. For the stationary planetary waves, a prominent example is SPW1, which can extend to high latitudes (beyond 60° MLAT), with larger amplitude in the winter hemisphere during solstice seasons. SPW3 and SPW4 are found to be much symmetric about the dip equator. As already mentioned above, DE1, D0, and DW2 are found to be the most prominent diurnal tidal components throughout the whole year. In general, these three tides are more favorable at middle to high latitudes. DE1 shows its largest values at northern midlatitudes, while D0 and DW2 are larger in the Southern Hemisphere. Smaller amplitude diurnal tides including DE3 and DE2 are more prominent at equatorial and low latitudes. DE3 is symmetric above the dip equator, while DE2 is found to be larger in the Southern Hemisphere. For the semidiurnal tides, SW1 and SW3 can extend to southern middle latitudes for most of the seasons except for December solstice, during which both of the two tidal components are confined to equatorial and low latitudes.

Figure 3 (right column) presents the seasonal and latitudinal variations of the nonmigrating tides (with different scale of amplitudes) during solar minimum periods. The seasonal and latitudinal variations of the tides are quite consistent with that during solar maximum periods, but the amplitudes of all the tides are reduced by a factor of about 2. Throughout the whole year, D0 and DW2 are found to be the most prominent tidal components at the southern midlatitudes, while DE1 is found to be dominant at northern midlatitude during equinoxes and June solstice. During September equinox, DE3 is found to be prominent at low latitudes, but with smaller amplitude compared to D0 and DW2 at middle latitudes.

4. Discussion

The analysis presented above has provided for the first time the electron density nonmigrating tidal spectrum on global scale for different seasons at both solar maximum and minimum conditions. The electron density observations from the CHAMP provide evidence for prominent nonmigrating tides at different latitude regions. These tides include diurnal components DE1, D0, and DW2, the semidiurnal components SW1 and SW3, as well as the planetary wave SPW1. Tidal components at equatorial and low latitudes can generally be related to be driven by equatorial electric fields.

4.1. Low-Latitude Tidal Signatures

When interpreting the spectral components we have to consider the local time dependence of the wave amplitudes. In our spectral analysis we have interpreted the whole 24 h of a day in one run. Therefore, signal from the tidal components, which are present only for part of a day, has leaked into other spectral components, and their physical interpretation requires special attention. *Teitelbaum and Vial* [1991] have investigated that effect in more detail. According to them the interacting parent waves (the tide and the local time modulation) produce child waves with frequencies and zonal wave numbers that are the sum and difference of the parent waves. The coupling mechanism we envisage is the equatorial ion fountain effect. This is driven by *E* layer zonal electric fields, and it transports plasma upward, thereby depleting the equatorial *F* region at the equator and accumulating plasma in the EIA crest regions. Any modulation of the *E* layer electric field is mapped with a certain time delay into the *F* region EIA [*Stolle et al.*, 2008]. A prominent feature in Figure 2 is the well-known WN4 longitudinal pattern in electron density at the crests of EIA. This can primarily be related to DE3 tide driving from below. Interestingly, the pattern is quite prominent during daytime hours but vanishes at late night and early morning hours. We interpret this as an indication for a wave driven by the *E* layer electric field. During night the *E* layer disappears and other mechanisms for interaction between ions and neutrals may appear in the *F* region.

A good proxy for the equatorial electric field is the strength of the EEJ. The recent paper by *Lühr and Manoj* [2013] presented the complete tidal spectrum of the EEJ. They also treated the problem of signal leaking into other components due to the confinement of the EEJ to daytime hours. The authors found DE3 as the most prominent tidal component during the months around August. Due to their processing approach about 30% of the actual DE3 signal has leaked into each of the child waves SPW4 and SE2 components. When inspecting our Figure 2 in the September equinox frame, we observe intense signal of DE3 and also appreciable amplitudes of SPW4 and SE2, in support of the leakage assumption. The same characteristic can be found although with smaller amplitudes in the June solstice frame. *Oberheide et al.* [2011] reported temperature and wind observations of SPW4 and SE2 tides in the middle atmosphere. These may contribute to the generation of the ionospheric SPW4 and SE2 signals. However, such a source cannot explain the

Table 1. The Amplitudes and Phases of the DE3, D0, and DW2 at EIA Crest (±20° MLAT) and Trough (0° MLAT) During September Equinox for Solar Maximum Period

September Equinox (2001–2002)						
	Northern Crest		Southern Crest		Trough at Dip Equator	
Tidal Components	Amplitude ($10^{10}m^{-3}$)	Phase (h)	Amplitude ($10^{10}m^{-3}$)	Phase (h)	Amplitude ($10^{10}m^{-3}$)	Phase (h)
DE3	12.14	13.81	10.29	15.21	6.32	1.37
D0	11.03	22.46	9.44	10.78	6.22	15.65
DW2	12.44	22.24	9.99	21.02	4.54	5.62

phase switch at the dip equator. Overall, the DE3 is not so dominant in the EIA as in the EEJ. We explain this by the short vertical wavelengths of DE3. Interestingly, the DE3 signal does not only appear at EIA crest latitudes but also right above the magnetic equator (see September equinox frame, left column). This signal is out of phase with crest variations by about 12 h (see phase values in Table 1). This means an enhancement of the crest is accompanied by a deep equatorial trough at CHAMP altitudes, in accordance with the electron density distribution shown in Figure 2.

Prominent WN3 signals at EIA crest latitudes present throughout the year can be related to the DE2 tide with some leakage into the SPW3 component [*Oberheide et al.*, 2011; *Xiong and Lühr*, 2013]. The tide DE2 has also been related to be driven by tropospheric processes and modulating of the *E* layer electric field.

The EEJ intensity is strongly modulated by a wave 2 longitudinal pattern related to SW4 during the months around December solstice as reported by *Lühr and Manoj* [2013] (see their Figure 17 and Table 4). Interestingly, we find no such SW4 signal for high solar activity but during solar minimum in the southern EIA crest regions. Also the expected leakage into the components, SPW2, DW3, and TW5 appear in that region.

During May and June the EEJ shows a prominent TW4 tidal signal [*Lühr and Manoj*, 2013]. Such a signal can also be found in the EIA (see our Figure 3) in the June solstice frame in particular during solar minimum conditions. As expected there is also a significant leakage into SW3 during that season.

As a further test for the origin of the low-latitude tidal components, we may compare the phases at the EIA crest with those at the trough. DE3 is prominent at equatorial and low-latitude regions during September equinox. According to Table 1, DE3 is out of phase (with 12 h difference) between the EIA crest (±20° MLAT) and the trough. We also compared the phases of the other components, DE2, D0, and DW2. Both DE2 and DW2 have almost the same phases at the two crests, but again about 12 h shifted values for DW2 at the trough, and about 18 h for DE2 (see Tables 1 and 2). Another interesting tidal component is SW3, which shows strong solar activity dependence [*Xiong and Lühr*, 2013]. From our Figure 3, we can see that it is symmetric about the dip equator and confined to low-latitude regions during December solstice for solar maximum conditions. The phase exhibits a difference between crest and trough of 6 h as listed in Table 2. We regard the antiphase behavior of the low-latitude tides as a strong evidence for the modulation of the EIA by the *E* layer zonal electric field. The coupling mechanism is the ion fountain effect.

An exception is the tidal component D0. It exhibits antiphase variations between the northern and southern crests (see Table 1). The same phase relation was already reported for D0 at middle latitudes by

Table 2. The Amplitudes and Phases of the DE2, DW2, and SW3 at EIA Crest (±20° MLAT) and Trough(0° MLAT) During December Solstice for Solar Maximum Period

December Solstice (2001–2002)						
	Northern Crest		Southern Crest		Trough at Dip Equator	
Tidal Components	Amplitude ($10^{10}m^{-3}$)	Phase (h)	Amplitude ($10^{10}m^{-3}$)	Phase (h)	Amplitude ($10^{10}m^{-3}$)	Phase (h)
DE2	3.48	22.32	9.45	20.17	2.26	3.32
DW2	12.26	21.52	10.22	21.95	7.48	7.58
SW3	7.41	7.64	7.70	7.63	10.21	1.13

Xiong and Lühr [2014]. At the EIA trough a phase is observed halfway between the northern and southern values. Explaining the peculiar behavior of D0 is beyond the scope of this paper.

4.2. Tidal Features at Middle and High Latitudes

As already revealed by previous studies, at equatorial and low-latitude regions the nonmigrating tides excited in the troposphere can propagate upward by direct propagation or through the *E* region wind dynamo coupling mechanism [*England et al.*, 2010; *Wu et al.*, 2012]. At middle latitudes other driving mechanisms have to be considered. In a recent paper *Xiong and Lühr* [2014] has presented various details of the electron density at midlatitudes during solstice seasons, showing that nonmigrating tides are also important at middle latitudes. At those zones no local time dependence of tidal activity has been reported. Thus, our spectra can be interpreted as they are and no leakage needs to be considered. This continuous wave activity over the whole day suggests an in situ excitation for the driving mechanism. We will return to this point in section 4.3.

The spectra presented in Figure 3 confirm all the features reported by *Xiong and Lühr* [2014], and here we have added the spectra for the equinoxes. Clearly dominating during all seasons is D0 at southern latitudes, which is generally accompanied by DW2. They suggested that the combination of these tidal components is the reason for the regional density anomalies, such as the Weddell Sea anomaly. In the Northern Hemisphere, DE1 takes over the leading role. Again in combination with D0, it causes diurnal varying regions of density anomaly. An interesting feature of D0 already reported by *Xiong and Lühr* [2014] and confined here is the variation in antiphase between the Northern and Southern Hemispheres. No such interhemispheric phase difference is observed for any of the other prominent tidal components. The origin of these nonmigrating components is believed to be an interaction between the dominant migrating tide and stationary planetary waves [*Jones et al.*, 2013] (see their Figures 4 and 5). In case of D0 and DW2 it could be the interaction between DW1 and SPW1. For DE1, a modulation of DW1 by SPW2 would be expected. Planetary waves reflect in our case primarily longitudinal dependent variations of the electron density, caused by the deflection of the magnetic equator from the geographic equator.

There are also semidiurnal tides at middle latitudes, e.g., SW1 and SW3. They are mainly confined to equinox seasons (except for SW3 in December solstice of solar maximum). This suggests that the semidiurnal migrating tide is larger during equinoxes, and there is a significant interaction between SPW1.

4.3. Comparison With Model Simulations

Until now there have only been a few attempts for disclosing the exact physical mechanisms of nonmigrating tides modulating the topside ionosphere at middle and high latitudes [e.g., *Chen et al.*, 2013]. Some mechanisms have been deduced from model simulations. A rather comprehensive study in that respect was presented by *Jones et al.* [2013]. The authors use the Thermosphere-Ionosphere-Mesosphere-Electrodynamics General Circulation Model to self-consistently simulate the dynamics of certain thermospheric parameters at altitudes close to our CHAMP heights (500 km for solar maximum, 350 km for solar minimum). The model considers a "realistic" geomagnetic field configuration (e.g., International Geomagnetic Reference Field 2010), and wave from the lower atmosphere can be fed into the lower boundary if desired. For their simulation runs they have chosen September equinox conditions. An important result is that the tidal components DE1, D0, and DW2 are most prominent in zonal wind. This is valid in particular at middle latitudes. Our observations confirm the dominance of these three diurnal components, at least for the electron density. In case of the semidiurnal tides *Jones et al.* [2013] reported SW1 and SW3 as the most important wind components. Likewise we find SW1 and SW3 being most prominent during equinox seasons (see Figure 3).

Jones et al. [2013] identified the ion-neutral interaction as the relevant mechanism for driving the tides in zonal wind at middle latitudes. We found the same tidal components in the CHAMP electron density observations, implying that the thermospheric winds may play an important role in driving ionospheric tides in the *F* region. *Jones et al.* [2013] reported the longitudinally varying ion-neutral friction, due to the actual geometry of the geomagnetic field, as the main cause for the nonmigrating tides. When the migrating tide DW1 interacts with the ion obstacle of type SPW1 or SPW2 modes like D0 and DW2 or DE1 and DW3 can be generated, respectively. Such tidal components are observed in electron density and predicted for the zonal wind. For explaining the nonmigrating tides SW1 and SW3 a semidiurnal migrating tide, SW2, is expected. SW2 seems to be stronger during equinox seasons according to our observations.

An interesting observation is that the well-known tidal components, like DE3 and SE2, show up in zonal wind, when the additional effects of tidal forcing of the model from the lower atmosphere are switched on. This confirms the role of the tides driven from the lower atmosphere. Also, our tidal observations at low latitudes could clearly be related to a driving by *E* layer electric field, and coupled through the ion fountain effect. There is one tidal component, D0, which does not fit the classification into low or middle latitudes. Different to the other tides it varies in antiphase between the two hemispheres, and the commonly observed phase flip between EIA crest and trough is not observed. A dedicated comparison of the prominent component D0 between observations and model simulations would be desirable.

5. Summary

In this study we present for the first time the electron density nonmigrating tidal spectrum in the topside ionosphere on global scale for different seasons and at both solar maximum and minimum conditions. The electron density observations from CHAMP satellite provide the evidence of nonmigrating tides at different latitude regions. A number of results were obtained.

1. DE1, D0, and DW2 are the primary tides that are believed to be driven by thermospheric winds through ion-neutral interactions. In general, these three diurnal tides appear preferably at middle and high latitudes during all the seasons. DE1 is only found in the northern middle and high latitudes, while D0 and DW2 are much stronger in the Southern Hemisphere. The envisaged excitation mechanism is an interaction of the migrating tide DW1 with the stationary SPW1 and SPW2.
2. At equatorial and low-latitude regions the most prominent diurnal tides are DE2 and DE3. DE2 is found to be present at low-latitude regions throughout the whole year, with larger amplitudes in the Southern Hemisphere, while DE3 shows its largest amplitude at the EIA crest region during September equinox. DE3 is symmetric above the dip equator, and the signal varies out of phase between the EIA crests and trough regions.
3. The semidiurnal tides SW1 and SW3 can also be found with smaller amplitudes throughout the whole year at low and middle latitudes. Interesting is the SW3 tide, which is confined to the equatorial and low-latitude regions during December solstices at solar maximum. During this season SW3 is also found to vary out of phase between the EIA crests and trough regions.
4. The tidal signature at low latitudes can be related to driving by *E* layer zonal electric fields. All the observed tidal components in the topside ionosphere are also found in the equatorial electrojet. The anticipated coupling mechanism is the ion fountain effect.
5. Somewhat special is D0. It varies in antiphase between the Northern and Southern Hemispheres. We have no immediate explanation for the type of mechanism that may be responsible. Study concerning special model effort is further needed.

In general, tides that cause the longitudinal wave 1 and wave 2 patterns are found to be more prominent at middle and high latitudes, such as SPW1, DE1, D0, DW2, SW1, and SW3, while tides that are related to longitudinal wave 3 and wave 4 patters are more favorable at equatorial and low-latitude regions, such as SPW3, SPW4, DE2, DE3, and SE2. These latter are caused by low atmospheric driving. Further study, in particular comparison between the in situ measurements and model simulations, is needed in order to understand the details of in situ generation and tropospheric wave excitation.

Acknowledgments

The CHAMP mission was sponsored by the Space Agency of the German Aerospace Center (DLR) through funds of the Federal Ministry of Economics and Technology. The CHAMP electron density measurement is available at the Information System and Data Center (ISDC) of GFZ German Research Centre for Geosciences (http://isdc.gfz-potsdam.de/modules.php?name=product_type_overview). The data set name is CH-ME-2-PLP. The work of Chao Xiong is supported by the Alexander von Humboldt Foundation through a Research Fellowship for Postdoctoral Researchers.

Alan Rodger thanks the reviewers for their assistance in evaluating this paper.

References

Angelats i Coll, M., and J. M. Forbes (2002), Nonlinear interactions in the upper atmosphere: The s = 1 and s = 3 nonmigrating semidiurnal tides, *J. Geophys. Res.*, *107*(A8), SIA 3-1–SIA 3-15, doi:10.1029/2001JA900179.

Chen, C. H., C. H. Lin, L. C. Chang, J. D. Huba, J. T. Lin, A. Saito, and J. Y. Liu (2013), Thermospheric tidal effects on the ionospheric midlatitude summer nighttime anomaly using SAMI3 and TIEGCM, *J. Geophys. Res. Space Physics*, *118*, 3836–3845, doi:10.1002/jgra.50340.

Emmert, J. T., A. D. Richmond, and D. P. Drob (2010), A computationally compact representation of Magnetic-Apex and Quasi-Dipole coordinates with smooth base vectors, *J. Geophys. Res.*, *115*, A08322, doi:10.1029/2010JA015326.

England, S. L., X. Zhang, T. J. Immel, J. Forbes, and R. DeMajistre (2009), The effect of non-migrating tides on the morphology of the equatorial ionospheric anomaly: Seasonal variability, *Earth Planets Space*, *61*, 493–503.

England, S. L., T. J. Immel, J. D. Huba, M. E. Hagan, A. Maute, and R. DeMajistre (2010), Modeling of multiple effects of atmospheric tides on the ionosphere: An examination of possible coupling mechanisms responsible for the longitudinal structure of the equatorial ionosphere, *J. Geophys. Res.*, *115*, A05308, doi:10.1029/2009JA014894.

Fesen, C. G., G. Crowley, R. G. Roble, A. D. Richmond, and B. G. Fejer (2000), Simulation of the pre-reversal enhancement in the low latitude vertical ion drifts, *Geophys. Res. Lett.*, *27*, 1851–1854, doi:10.1029/2000GL000061.

Forbes, J. M., J. Russell, S. Miyahara, X. Zhang, S. Palo, M. Mlynczak, C. J. Mertens, and M. E. Hagan (2006), Troposphere-thermosphre tidal coupling as measured by the SABER instrument on TIMED during July-September 2002, *J. Geophys. Res.*, *111*, A10S06, doi:10.1029/2005JA011492.

Hagan, M. E., and J. M. Forbes (2002), Migrating and nonmigrating diurnal tides in the middle and upper atmosphere excited by tropospheric latent heat release, *J. Geophys. Res.*, *107*(D24), 4754, doi:10.1029/2001JD001236.

Hagan, M. E., A. Maute, and R. G. Roble (2009), Tropospheric tidal effects on the middle and upper atmosphere, *J. Geophys. Res.*, *114*, A01302, doi:10.1029/2008JA013637.

Häusler, K., and H. Lühr (2009), Nonmigrating tidal signals in the upper thermospheric zonal wind at equatorial latitudes as observed by CHAMP, *Ann. Geophys.*, *27*, 2643–2652.

Immel, T. J., E. Sagawa, S. L. England, S. B. Henderson, M. E. Hagan, S. B. Mende, H. U. Frey, C. M. Swenson, and L. J. Paxton (2006), Control of equatorial ionospheric morphology by atmospheric tides, *Geophys. Res. Lett.*, *33*, L15108, doi:10.1029/2006GL026161.

Jones, M., Jr., J. M. Forbes, M. E. Hagan, and A. Maute (2013), Non-migrating tides in the ionosphere-thermosphere: In situ versus tropospheric sources, *J. Geophys. Res. Space Physics*, *118*, 2438–2451, doi:10.1002/jgra.50257.

Kil, H., S.-J. Oh, M. C. Kelley, L. J. Paxton, S. L. England, E. Talaat, K.-W. Min, and S.-Y. Su (2007), Longitudinal structure of the vertical E×B drift and ion density seen from ROCSAT-1, *Geophys. Res. Lett.*, *34*, L14110, doi:10.1029/2007GL030018.

Lühr, H., M. Rother, K. Häusler, P. Alken, and S. Maus (2008), The influence of non-migrating tides on the longitudinal variation of the equatorial electrojet, *Geophys. Res. Lett.*, *113*, A08313, doi:10.1029/2008JA013064.

Lühr, H., M. Rother, K. Häusler, B. Fejer, and P. Alken (2012), Direct comparison of non-migrating tidal signatures in the electrojet, vertical plasma drift and equatorial ionization anomaly, *J. Atmos. Sol. Terr. Phys.*, *75–76*, 31–43, doi:10.1016/j.jastp.2011.07.009.

Lühr, H., and C. Manoj (2013), The complete spectrum of the equatorial electrojet related to solar tides: CHAMP observations, *Ann. Geophys.*, *31*, 1315–1331, doi:10.5194/angeo-31-1315-2013.

McNamara, L., D. L. Cooke, C. E. Valladares, and B. W. Reinisch (2007), Comparison of CHAMP and digisonde plasma frequencies at Jicamarca, Peru, *Radio Sci.*, *42*, RS2005, doi:10.1029/2006RS003491.

Oberheide, J., Q. Wu, T. L. Killeen, M. E. Hagan, and R. G. Roble (2006), Diurnal nonmigrating tides from TIMED Doppler Interferometer wind data: Monthly climatologies and seasonal variations, *J. Geophys. Res.*, *111*, A10S03, doi:10.1029/2005JA011491.

Oberheide, J., J. M. Forbes, X. Zhang, and S. L. Bruinsma (2011), Wave-driven variability in the ionosphere-thermosphere-mesosphere system from TIMED observations: What contributes to the "wave 4", *J. Geophys. Res.*, *116*, A01306, doi:10.1029/2010JA015911.

Pancheva, D., Y. Miyoshi, P. Mukhtarov, H. Jin, H. Shinagawa, and H. Fujiwara (2012), Global response of the ionosphere to atmospheric tides forced from below: Comparison between COSMIC measurements and simulations by atmosphere-ionosphere coupled model GAIA, *J. Geophys. Res.*, *117*, A07319, doi:10.1029/2011JA017452.

Park, J., H. Lühr, B. G. Fejer, and K. W. Min (2010), Duskside F-region dynamo currents: Its relationship with prereversal enhancement of vertical plasma drift, *Ann. Geophys.*, *28*, 2097–2101, doi:10.5194/angeo-28-2097-2010.

Reigber, C., H. Lühr, and P. Schwintzer (2002), CHAMP mission status, *Adv. Space Res.*, *30*, 129–134.

Scherliess, L., D. C. Thompson, and R. W. Schunk (2008), Longitudinal variability of low- latitude total electron content: Tidal influences, *J. Geophys. Res.*, *113*, A01311, doi:10.1029/2007JA012480.

Stolle, C., C. Manoj, H. Lühr, S. Maus, and P. Alken (2008), Estimating the daytime equatorial ionization anomaly strength from electric field proxies, *J. Geophys. Res.*, *113*, A09310, doi:10.1029/2007JA012781.

Teitelbaum, H., and F. Vial (1991), On tidal variability induced by nonlinear interaction with planetary waves, *J. Geophys. Res.*, *96*(A8), 14,169–14,178, doi:10.1029/91JA01019.

Wan, W., J. Xiong, Z. Ren, L. Liu, M.-L. Zhang, F. Ding, B. Ning, B. Zhao, and X. Yue (2010), Correlation between the ionospheric WN4 signature and the upper atmospheric DE3 tide, *J. Geophys. Res.*, *115*, A11303, doi:10.1029/2010JA015527.

Woodman, R. F. (1970), Vertical drift velocities and east-west electric fields at the magnetic equator, *J. Geophys. Res.*, *75*(31), 6249–6259, doi:10.1029/JA075i031p06249.

Wu, Q., D. A. Ortland, B. Foster, and R. G. Roble (2012), Simulation of nonmigrating tide influences on the thermosphere and ionosphere with a TIMED data driven TIEGCM, *J. Atmos. Sol. Terr. Phys.*, *90–91*, 61–67, doi:10.1016/j.jastp.2012.02.009.

Xiong, C., and H. Lühr (2013), Nonmigrating tidal signatures in the magnitude and the inter-hemispheric asymmetry of the equatorial ionization anomaly, *Ann. Geophys.*, *31*, 1115–1130, doi:10.5194/angeo-31-1115-2013.

Xiong, C., and H. Lühr (2014), The midlatitude summer night anomaly as observed by CHAMP and GRACE: Interpreted as tidal features, *J. Geophys. Res. Space Physics*, *119*, 4905–4915, doi:10.1002/2014JA019959.